Science Signaling
AAAS

` A Systems Approach for Decoding Mitochondrial Retrograde Signaling Pathways

Sehyun Chae, Byung Yong Ahn, Kyunghee Byun, Young Min Cho, Myeong-Hee Yu, Bonghee Lee, Daehee Hwang and Kyong Soo Park (26 February 2013)
Science Signaling **6** (264), rs4. [DOI: 10.1126/scisignal.2003266]

Science Signaling (ISSN 1937-9145) is published weekly, except the last week in December, by the American Association for the Advancement of Science, 1200 New York Avenue, NW, Washington, DC 20005.

CELL BIOLOGY

A Systems Approach for Decoding Mitochondrial Retrograde Signaling Pathways

Sehyun Chae,[1,2*] Byung Yong Ahn,[2*] Kyunghee Byun,[3*] Young Min Cho,[2] Myeong-Hee Yu,[4] Bonghee Lee,[3†] Daehee Hwang,[1,5,6†] Kyong Soo Park[2†]

Mitochondrial dysfunctions activate retrograde signaling from mitochondria to the nucleus. To identify transcription factors and their associated pathways that underlie mitochondrial retrograde signaling, we performed gene expression profiling of the cells engineered to have varying amounts of mitochondrial DNA with an A3243G mutation (mt3243) in the leucine transfer RNA ($tRNA^{Leu}$), which reduces the abundance of proteins involved in oxidative phosphorylation that are encoded by the mitochondrial genome. The cells with the mutation exhibited reduced mitochondrial function, including compromised oxidative phosphorylation, which would activate diverse mitochondrial retrograde signaling pathways. By analyzing the gene expression profiles in cells with the mutant $tRNA^{Leu}$ and the transcription factors that recognize the differentially regulated genes, we identified 72 transcription factors that were potentially involved in mitochondrial retrograde signaling. We experimentally validated that the mt3243 mutation induced a retrograde signaling pathway involving RXRA (retinoid X receptor α), reactive oxygen species, kinase JNK (c-JUN N-terminal kinase), and transcriptional coactivator PGC1α (peroxisome proliferator–activated receptor γ, coactivator 1 α). This RXR pathway contributed to the decrease in mRNA abundances of oxidative phosphorylation enzymes encoded in the nuclear genome, thereby aggravating the dysfunction in oxidative phosphorylation caused by the reduced abundance of mitochondria-encoded enzymes of oxidative phosphorylation. Thus, matching transcription factors to differentially regulated gene expression profiles was an effective approach to understand mitochondrial retrograde signaling pathways and their roles in mitochondrial dysfunction.

INTRODUCTION

Impaired mitochondrial functions affect the amount of cytosolic Ca^{2+}, reactive oxygen species (ROS), or adenosine monophosphate (AMP), and the changes in these cytosolic constituents can activate diverse retrograde signaling pathways from the mitochondria to the nucleus. This mitochondrial retrograde signaling changes the activities of various nuclear transcription factors (TFs; table S1) and, thus, the abundances of their target genes, thereby affecting cellular processes, such as growth, proliferation, apoptosis, metabolism, or mitochondrial biogenesis (*1*–*6*). The components in retrograde signaling pathways that are activated by mitochondrial dysfunctions are mostly unknown.

Systems biology approaches have been used to investigate the complex and diverse mitochondrial retrograde signaling mechanisms. Systems biology approaches involve the identification of genes and cellular processes perturbed by mitochondrial dysfunctions and the generation of network models for identifying retrograde signaling pathways activated by the perturbation (*7*). Gene expression analysis of muscle tissues from three different groups of patients with (i) mitochondrial encephalomyopathy, lactic acidosis, and stroke-like episodes ($MELAS^{A3243G}$) associated with the mitochondrial leucine transfer RNA ($tRNA^{Leu}$; A3243G) mutation (mt3243 mutation); (ii) progressive external ophthalmoplegia (PEO^{A3243G}) associated with the mt3243 mutation; and (iii) PEO associated with mitochondrial DNA (mtDNA) macrodeletions showed that mRNA abundances of 56 and 31 genes were changed by mt3243 and mtDNA macrodeletion mutations, respectively (*8*). These genes are involved in oxidative phosphorylation (OXPHOS), protein biosynthesis, metabolism, transcription, signal transduction, and cell cycle. However, these studies were unable to identify retrograde signaling pathways through which these genes were regulated.

Here, we present a systems biology approach to identify retrograde signaling pathways. To demonstrate use of this approach, we performed gene expression profiling of cells engineered with varying amounts of mtDNAs with the mt3243 mutation, cells with none of the mutant mtDNA, cells with some of the mutant mtDNA, and cells with only the mutant mtDNA. The mt3243 mutation in the $tRNA^{Leu}$ gene reduces protein synthesis in mitochondria, leading to decreased abundances of mitochondrial-encoded OXPHOS enzymes (*9*, *10*), reduced OXPHOS, and activation of diverse retrograde signaling pathways (*3*, *6*). With the gene expression profiles, we identified 72 potential TFs involved in retrograde signaling induced by the mt3243 mutation. We showed that retinoid X receptor α (RXRA) participated in a retrograde signaling pathway induced by the mt3243 mutation. This pathway also involved ROS, c-JUN N-terminal kinase (JNK), and a peroxisome proliferator–activated receptor γ, coactivator 1 α (PGC1α) and contributed to the decrease in mRNA abundances of nuclear-encoded OXPHOS enzymes, which would further aggravate OXPHOS dysfunction caused by the mt3243 mutation. Although the negative regulation of RXRA abundance through JNK activated by ROS (*11*)

[1]School of Interdisciplinary Bioscience and Bioengineering, Pohang University of Science and Technology, Pohang 790-784, Republic of Korea. [2]Department of Internal Medicine, Seoul National University College of Medicine, Seoul 110-799, Republic of Korea. [3]Center for Genomics and Proteomics & Stem Cell Core Facility, Lee Gil Ya Cancer and Diabetes Institute, Gachon University of Medicine and Science, Incheon 406-799, Republic of Korea. [4]Korea Institute of Science and Technology, Seoul 136-791, Republic of Korea. [5]Department of Chemical Engineering, Pohang University of Science and Technology, Pohang 790-784, Republic of Korea. [6]Integrative Biosciences and Biotechnology, Pohang University of Science and Technology, Pohang 790-784, Republic of Korea.
*These authors contributed equally to this work.
†To whom correspondence should be addressed. E-mail: dhhwang@postech.ac.kr (D.H.); kspark@snu.ac.kr (K.S.P.); bhlee@gachon.ac.kr (B.L.)

and the interaction between RXRA and PGC1α (*12*) have been previously reported, the connection of this pathway to mitochondrial retrograde signaling has not. Here, we demonstrated that (i) mitochondrial dysfunctions decreased RXRA abundance, (ii) the reduction in RXRA decreased the interaction between RXRA and PGC1α, (iii) the reduced interaction contributed to the decrease in mRNA abundances of OXPHOS and translation-related genes, and (iv) the reduction of OXPHOS and translation-related genes was reversed by the addition of retinoic acid (RA).

RESULTS

Mitochondrial dysfunctions in cybrid cells carrying the mt3243 mutation

To investigate retrograde signaling pathways induced by the mitochondrial dysfunction caused by the mt3243 mutation, we generated three types of cybrid cells using a mitochondria-mediated transformation method (*10*). Cells lacking mtDNA were fused with mtDNAs with the mt3243 mutation isolated from platelets of a diabetic patient with sensorineural hearing loss. We determined the proportion of wild-type and mutant mtDNA of cybrid cells by polymerase chain reaction (PCR)–restriction fragment length polymorphism (RFLP) analysis using mtDNA probe (Fig. 1A). We then isolated three types of cybrid cells: W cells had wild-type mtDNA (3243A homoplasmy), H cells had both the mutant and wild-type mtDNA (3243A/G heteroplasmy) with 70% of the mtDNA containing 3243G, and M cells had only mutant mtDNA (3243G homoplasmy). To confirm mitochondrial dysfunctions caused by the mt3243 mutation, we measured O_2 consumption and relative adenosine 5′-triphosphate (ATP) content in the three types of cybrid cells. In H and M cells, both O_2 consumption and ATP content were significantly decreased compared to W cells (Fig. 1, B and C), consistent with findings in previous studies (*9*, *10*, *13*). We also examined the abundances of representative enzymes of the five OXPHOS complexes (Fig. 1D). In H and M cells, the amounts of these enzymes were reduced. Furthermore, the activity of cytochrome c oxidase in the OXPHOS complex IV was decreased in the H and M cells (Fig. 1E). These data indicate that the mt3243 mutation induced OXPHOS dysfunctions by reducing both amounts and activities of OXPHOS enzymes.

Alteration of mRNA abundances caused by the mt3243 mutation

The OXPHOS dysfunction caused by the mt3243 mutation activates retrograde signaling pathways, resulting in alteration of nuclear gene expression. We performed gene expression profiling of the three types of cybrid cells (W, H, and M cells) and then compared mRNA abundances between the different types of cybrid cells—H versus W, M versus W, and M versus H. We identified 2404 differentially expressed genes (DEGs) with false discovery rate (FDR) less than 0.05 and fold change larger than 1.46 (Materials and Methods) in at least one of the three comparisons (Fig. 2A). These DEGs encode proteins that are involved in cellular processes previously shown to be affected by the mt3243 mutation (fig. S1A). Also, among the 56 genes previously reported to be affected by the mt3243 mutation (*8*), 19 genes are shared with the 2404 DEGs ($P < 10^{-6}$; fig. S1B). Large numbers of DEGs were identified from the comparisons of M versus W and M versus H (1687 and 1350 DEGs, respectively), whereas only 540 DEGs were identified from the comparison of H versus W. These data indicate that gene expression can be significantly altered by the single point mutation in a mutation load–dependent manner.

The mt3243 mutation primarily compromises OXPHOS, which can then perturb multiple cellular processes (*14*–*16*). To systematically investigate these processes, we categorized the 2404 DEGs into 26 clusters based on their differential expression patterns (tables S2 and S3). Among the 26 clusters, we focused on 12 clusters (Fig. 2B), each of which included at least more than 25 genes (1% of the total number of DEGs; table S2). We identified cellular processes represented by the genes in the individual clusters by performing enrichment analysis of Gene Ontology (GO) Biological Processes using DAVID software (*17*) (Fig. 2C and table S4). The analysis revealed that the genes affected by the mt3243 mutation are mainly involved in mitochondrial processes (mitochondrial transport, mitochondrion organization, OXPHOS, responses to ROS and oxidative stress, and nitrogen compound biosynthetic process), protein homeostasis–related processes (translation, ribosome biogenesis, protein transport, and regulation of protein ubiquitination), and cell proliferation–related processes

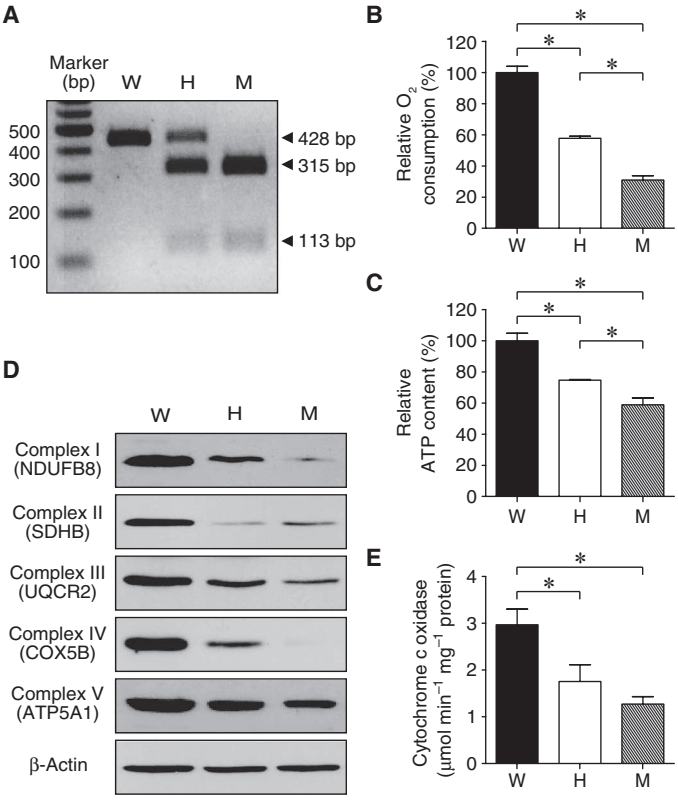

Fig. 1. Reduction of OXPHOS complex activity caused by the mt3243 mutation in cybrid cells. (**A**) Degree of heteroplasmy of the mutant (3243G) mtDNA of three types of cybrid cells—W (0%), H (70%), and M (100%). Data are representative of three independent experiments. Oligonucleotide primers were designed to amplify mtDNA encompassing the mutated site from 3130 to 3558 to generate 428-bp (base pair) PCR products. With the treatment of *Apa-I* that cleaves specifically the A3243G mutation, the H and M cells resulted in fragments of 315 and 113 bp, whereas the W cells have the intact 428-bp PCR products. (**B** and **C**) Relative basal oxygen consumption (B) and ATP content (C) of the three types of cybrid cells; $n = 3$ independent experiments. (**D**) Abundances of representative enzymes in OXPHOS complexes I to V in three types of cybrid cells. Data are representative of three independent experiments. (**E**) Activity of cytochrome c oxidase in three types of cybrid cells; $n = 3$ independent experiments. The data are shown as means ± SD; $^*P < 0.05$ by one-way analysis of variance (ANOVA) with Bonferroni correction (B, C, and E).

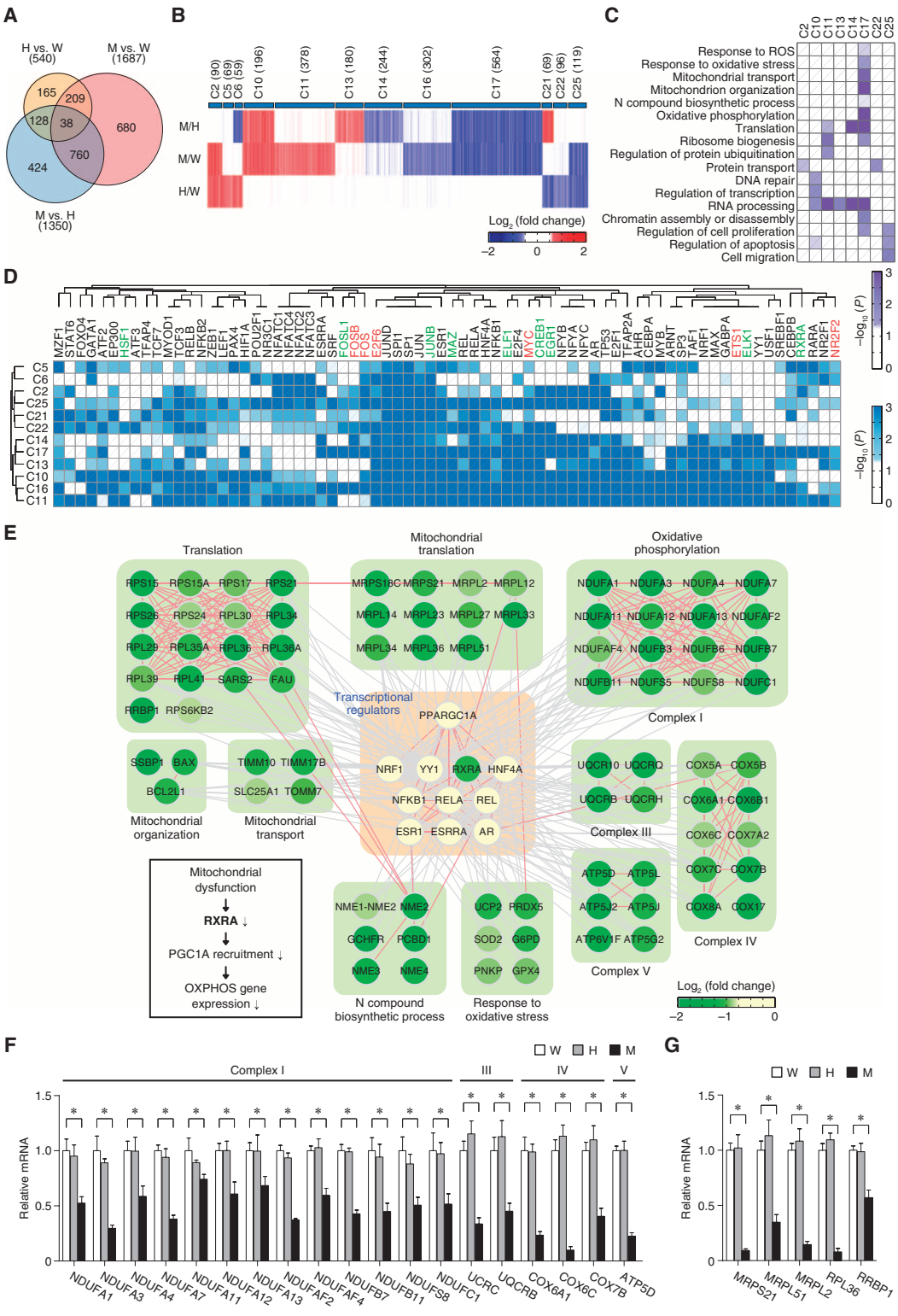

Fig. 2. Differentially regulated genes and the 72 TFs implicated in mitochondrial retrograde signaling. (**A**) Relationships among DEGs in three cybrid cells. Numbers in parenthesis, total numbers of DEGs in each indicated comparison. (**B**) Differential expression of genes in the 12 major clusters from the original 26 clusters. Number of genes in each cluster is indicated in parentheses (see table S2 for complete list of clusters and the numbers of genes in each; see table S3 for a complete list of genes in each cluster). (**C**) GO Biological Processes enrichment of genes in the indicated 12 clusters. Color bar, gradient of $-\log_{10}(P)$; *P*, enrichment *P* value. (**D**) Seventy-two TF candidates and the distributions of their targets in the indicated 12 clusters. Color bar, gradient of $-\log_{10}(P)$; *P*, significance of each cluster being enriched in targets of individual TFs. TFs written in red and green represent TFs that had increased or decreased mRNA abundance, respectively, in cells with higher mutation loads, compared to cells with lower mutation loads (that is, H versus W, M versus W, or M versus H). Dendrograms show similarity between TFs (or clusters) based on their target distributions. (**E**) A network model delineating relationships between PGC1α-interacting TFs (center peach-shaded box) and their target genes (green-shaded boxes). Edges, TF-target (gray) and protein-protein interactions (red). Color bar, gradient of $\log_2$ fold changes in mRNA abundance for the nodes in M versus W. (**F** and **G**) qRT-PCR analysis of OXPHOS and translation-related genes; $n = 5$ independent experiments. Data are normalized against expression of glyceraldehyde-3-phosphate dehydrogenase (GAPDH) and shown as means ± SD; $^*P < 0.05$ by one-way ANOVA with Bonferroni correction.

(regulation of cell proliferation, DNA repair, regulation of apoptosis, regulation of transcription, chromatin assembly or disassembly, and RNA processing). The results showed that the mitochondrial dysfunction caused by the single point (mt3243) mutation affects a broad spectrum of cellular processes, likely reflecting the activation of diverse retrograde signaling pathways that alter these cellular processes.

Potential TFs regulating alteration of mRNA abundances by the mt3243 mutation

Several signaling pathways and their downstream TFs (table S1) have been implicated in mitochondrial retrograde signaling. To investigate retrograde signaling pathways activated by the mt3243 mutation, we identified potential downstream TFs that could contribute to the alteration of gene expression in the selected 12 clusters (Fig. 2B) (Materials and Methods). Briefly, for the 799 TFs with reported targets, we counted the numbers of their targets in the individual DEG clusters using the 223,665 TF-target interactions from MetaCore and five protein-DNA interactome databases (table S5). We then selected the 72 TFs with significant numbers of targets (FDR < 0.01) in the 12 clusters as TF candidates that could be involved in retrograde signaling (Fig. 2D and table S6A; Materials and Methods). The large number of the candidates (72 TFs) indicated that the mitochondrial dysfunction caused by the mt3243 mutation induced diverse retrograde signaling pathways. Of 72 TFs, 26 are involved in known retrograde signaling pathways (table S6B). Furthermore, the mRNA abundances of 15 of 72 TFs were increased or decreased in cells with higher mutation loads, compared to cells with lower mutation loads (H versus W, M versus W, or M versus H): mRNA abundances of NR2F2, ETS1, FOSB, FOS, E2F6, and MYC were increased, and the abundances of HSF1, RXRA, MAZ, ELK1, ELF1, CREB1, EGR1, FOSL1, and JUNB were decreased (table S6B). Among the 15 TFs, 7 (FOSB, FOS, MYC, CREB1, EGR1, FOSL1, and JUNB) have been reported to be involved in mitochondrial retrograde signaling (fig. S2 and table S6B).

Retrograde signaling TFs regulating mRNA abundances of OXPHOS genes

Changes in the mRNA abundances of the genes encoding OXPHOS enzymes are a well-known feature of mitochondrial dysfunctions (*18*). Depending on the severity and types of mitochondrial dysfunctions, mRNA abundances of OXPHOS genes may increase (*8*, *19*) or decrease (*20*, *21*). Here, among the 46 OXPHOS genes altered by the presence of the mt3243 mutation, mRNA abundances of 44 were decreased (table S7). The decreased mRNA abundances resulted in the reduction in the protein abundances of nuclear-encoded OXPHOS enzymes (Fig. 1D), which would serve as a positive feedback loop to enhance the OXPHOS dysfunction caused by the reduction in the abundances of mitochondrial-encoded OXPHOS enzymes due to the mt3243 mutation. Thus, mitochondrial retrograde signaling leading to the decrease in mRNA abundances of nuclear-encoded OXPHOS genes contributed to the OXPHOS dysfunctions induced by the presence of the mt3243 mutation.

The enrichment analysis of Gene Ontology Biological Processes (Fig. 2C) showed that, among the 12 clusters, genes associated with OXPHOS were most significantly represented in cluster 17 (C17), and this included the genes with mRNA abundances that were decreased in M cells, but not in H cells (Fig. 2B). Among the 46 OXPHOS genes altered by the presence of the mt3243 mutation (table S7), 36 genes belonged to C17. To identify the retrograde signaling pathways that altered the expression of the genes in C17, we identified 52 candidate TFs that had significant numbers of targets in C17 (FDR < 0.01; Materials and Methods; table S6A and Fig. 2D). Ten of the 52 TFs (AR, ESR1, ESRRA, HNF4A, NKFB1, NRF1, REL, RELA, RXRA, and YY1) form transcriptional regulatory complexes with PGC1α (PPARGC1A) (table S6B), a major regulator of OXPHOS and mitochondrial biogenesis (*22*–*24*). The data indicated that PGC1α-TF complexes can contribute to the decrease in mRNA abundances of the genes in C17.

To investigate which of the processes represented by the genes in C17 (Fig. 2C) are regulated by the PGC1α-interacting TFs, we reconstructed a network model using the PGC1α-interacting TFs and their target genes in C17 (Fig. 2E). The network revealed that these 10 TFs primarily regulated C17 target genes classified as mitochondrial processes, including OXPHOS, and as translation. Among the 10 PGC1α-interacting TFs, only the gene encoding RXRA, which is a gene in C17, exhibited decreased expression in the presence of the mt3243 mutation. Ligand-stimulated RXRA recruits PGC1α to RA response elements in the promoters of target genes, and PGC1α functions as a coactivator to promote the transcriptional activity of RXRA (*12*, *25*, *26*). 9-*Cis*-RA induces expression of mitochondria-related genes (*27*–*29*). Thus, we hypothesized that the decreased RXRA abundance could reduce the recruitment of PGC1α, leading to the decrease in expression of OXPHOS genes and enhanced mitochondrial dysfunction (Fig. 2E, inset). To confirm the gene expression data, we analyzed by quantitative reverse transcriptase PCR (qRT-PCR) analysis 19 of the OXPHOS genes (Fig. 2F) and 5 of the translation- and mitochondrial translation–related genes (Fig. 2G) in the network model (Fig. 2E) and showed that their mRNA abundances were decreased in M cells, but not in H cells, compared to W cells, consistent with the differential expression pattern of C17.

Restoration of OXPHOS genes by increasing transcriptional activity of RXRA

To experimentally test if reduced RXRA abundance contributed to the decrease in OXPHOS gene expression, we confirmed both the decreased mRNA and protein abundances of RXRA in M cells (Fig. 3A). To examine a functional role for RXRA in regulating mRNA abundances of OXPHOS genes, we treated H and M cells with RA and found that both O_2 consumption and ATP content, which were decreased by the mt3243 mutation (Fig. 1, B and C), were significantly restored in RA-treated H and M cells (Fig. 3B), although the restoration of O_2 consumption did not reach that of the control, untreated W cells. Furthermore, the abundances of several OXPHOS enzymes were restored closely to those in W cells (Fig. 3C).

Of the 564 genes in C17 that were decreased in M cells by the mt3243 mutation (Fig. 2B), we found that 163 genes were restored in their mRNA abundances (FDR < 0.05) by RA treatment of M cells (Fig. 3D and table S8). The enrichment analysis of GO Biological Processes of the 163 genes (Fig. 3E) showed that these are mainly associated with OXPHOS, mitochondrial transport, and the response to oxidative stress ($P < 0.05$), indicating that these processes were restored among the mitochondrial processes represented by the genes in C17 (Fig. 2E). Among the 36 OXPHOS genes in C17, 10 were restored in their mRNA abundances. To verify that the OXPHOS genes were regulated by RXRA, we knocked down RXRA with short-interfering RNA (siRNA) in W cells (fig. S3) and then measured the mRNA abundances of the 10 OXPHOS genes. The mRNA abundances of the 10 genes were decreased by knockdown of RXRA, indicating that the 10 OXPHOS genes are regulated by RXRA (Fig. 3F). Thus, the decrease in RXRA contributed to the decrease in mRNA abundances of OXPHOS genes.

Restoration of OXPHOS gene expression by increasing the RXRA-PGC1α interaction

To investigate if the reduction in RXRA decreased the amount of RXRA-PGC1α complexes and thus inhibited expression of OXPHOS genes, we tested whether inducing the RXRA-PGC1α interaction would restore mRNA abundances of OXPHOS genes. We measured the RXRA-PGC1α interaction in cybrid cells after RA treatment using a proximity ligation assay (PLA; Materials and Methods). In M cells, RA treatment increased significantly RXRA-PGC1α interaction in the nucleus (Fig. 4A), whereas RA treatment did not significantly change in the amount of the interaction in W or H cells, which is consistent with the finding that mRNA

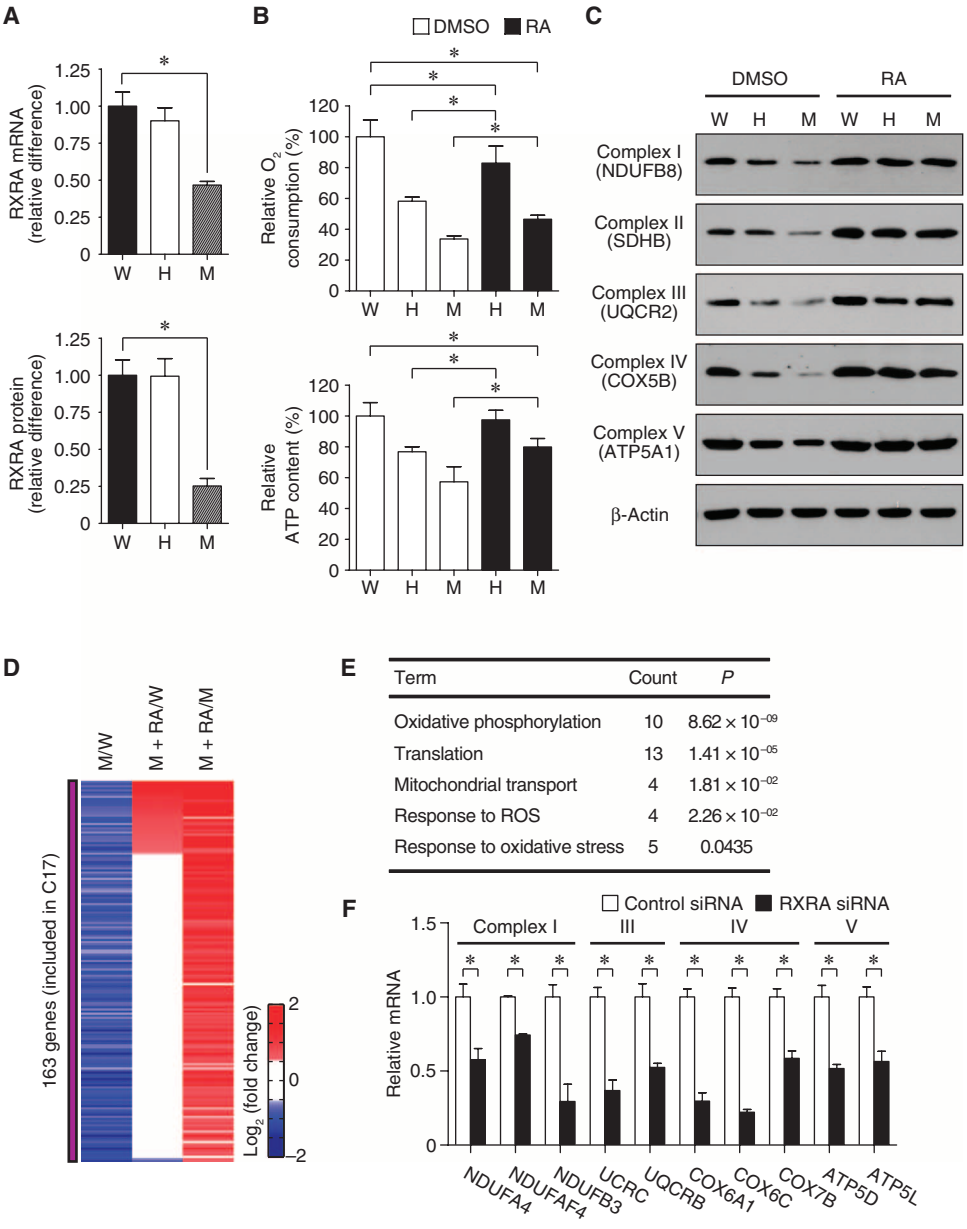

Fig. 3. Restoration of expression of OXPHOS genes by RA treatment. (**A**) qRT-PCR analysis and Western blotting analysis of RXRA mRNA and protein abundance in three types of cybrid cells; $n = 5$ independent experiments for RT-PCR and $n = 3$ independent experiments for Western blotting; $^*P < 0.05$ by one-way ANOVA with Bonferroni correction. (**B**) Relative oxygen consumption and ATP content of the three types of cybrid cells with or without treatment with 10 μM RA for 24 hours; $n = 5$ independent experiments; $^*P < 0.05$ by two-way ANOVA with Bonferroni correction. (**C**) Western blotting analysis of representative enzymes of OXPHOS complexes I to V in three types of cybrid cells with and without the RA treatment. Data are representative of three independent experiments. (**D**) Gene expression patterns of 163 genes that exhibited increased mRNA abundance in M cells treated with RA treatment. (**E**) GO Biological Processes enrichment of the 163 genes. Count, number of genes involved in each process among the 163 genes; *P*, enrichment *P* values from DAVID. (**F**) qRT-PCR analysis of OXPHOS genes in control siRNA–transfected and RXRA siRNA–transfected W cells. Transcript abundance was normalized to that of GAPDH; $n = 5$ independent experiments; $^*P < 0.05$ compared with control siRNA condition for each gene by Student's *t* test. Quantified data are shown as means ± SD.

abundances of the OXPHOS genes in C17 were not altered in H cells (Fig. 2B). This suggested that RXRA may act as a sensor of the mitochondrial dysfunction caused by the mutation load.

To test if the RXRA-PGC1α interaction regulated the mRNA abundances of OXPHOS genes, we transfected M cells with FK506 binding protein (FKBP)–RXRA and FKBP-rapamycin binding domain (FRB) fusion vectors after silencing wild-type RXRA in M cells using siRNA, as previously described (*30*). FRB is localized to the plasma membrane. Rapamycin treatment induces the interaction between FKBP-RXRA and FRB, thereby moving FKBP-RXRA to the plasma membrane and thus reducing the interaction of FKBP-RXRA with PGC1α in the nucleus. When the interaction between FKBP-RXRA and PGC1α was reduced by rapamycin treatment, the RA treatment failed to restore mRNA abundances of the OXPHOS genes in M cells (Fig. 4B). The RA-induced interaction data and the sequestration data are consistent with the model that RA treatment induced an increase in RXRA-PGC1α complexes, and this contributed to the restoration of OXPHOS gene expression in M cells.

Negative regulation of mRNA abundance of RXRA through JNK activated by ROS

Our data indicated that the reduction in RXRA contributed to the decreased mRNA abundances of the OXPHOS genes. Diverse mitochondrial retrograde signaling pathways initiated by mitochondrial dysfunction involve changes in Ca^{2+}, ROS, and AMP. Among these mediators, ROS decreases both mRNA and protein abundances of RXRA in neonatal rat cardiomyocytes (*11*). Thus, we measured the amounts of ROS in the three types of cybrid cells. The relative amount of ROS was increased in H and M cells (Fig. 5A). To determine whether increased ROS reduced the abundance of RXRA, we measured mRNA and protein abundances of RXRA after treating the cybrid cells with ascorbic acid, an antioxidant that decreases the amount of ROS in cells (Fig. 5B). In M cells, both the mRNA and protein abundances of RXRA were restored, and protein abundance exceeded that of control W cells, indicating that the increased ROS contributed to reducing the RXRA abundance. In contrast, H cells, which did not have much difference from W cells in the abundance of RXRA protein (Figs. 3A and 5B), also did not show a significant change

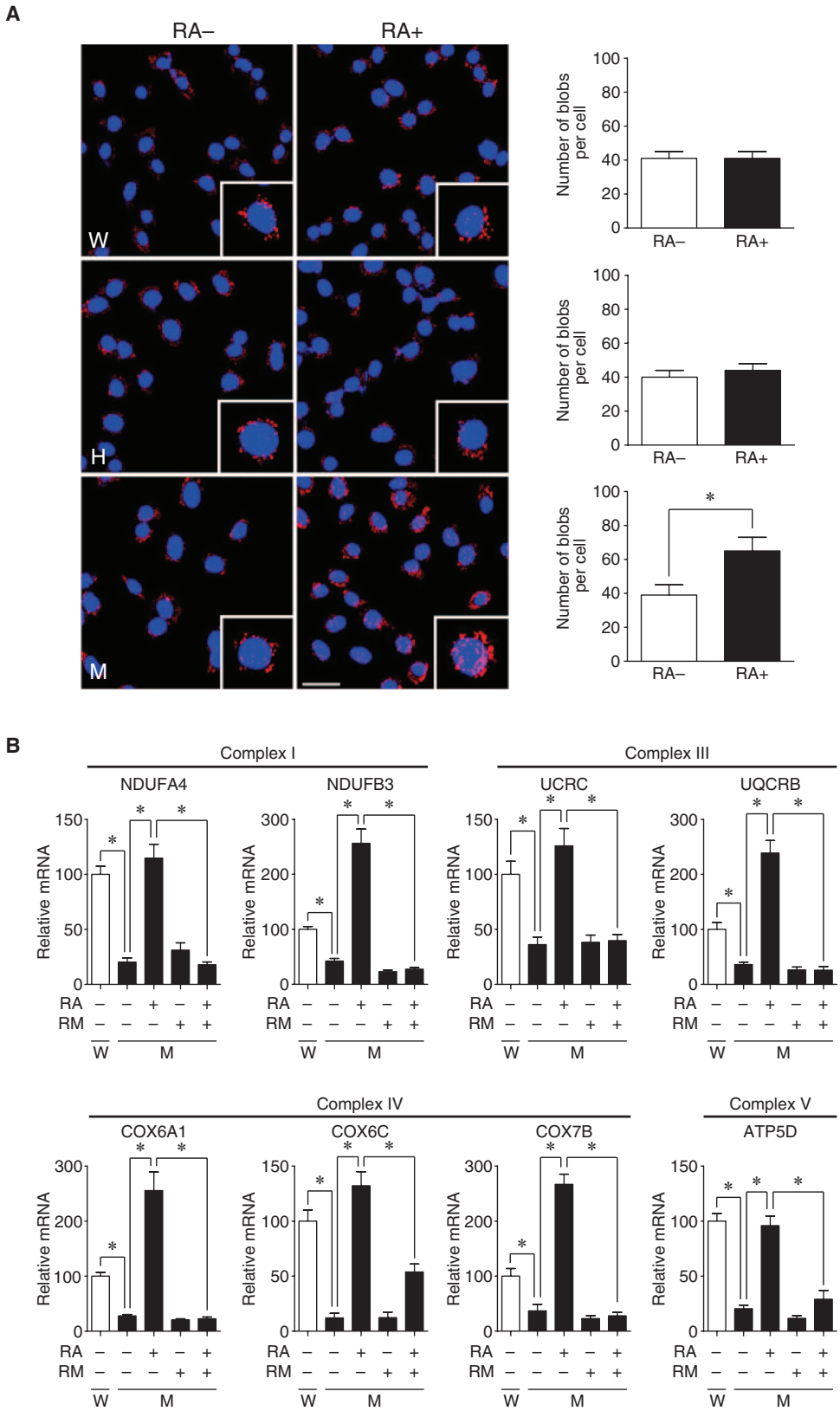

Fig. 4. Restoration of expression of OXPHOS genes by increasing the RXRA-PGC1α interaction. (**A**) PLA to measure RXRA-PGC1α interactions (red puncta or blobs) in the three types of cybrid cells with (RA+) and without (RA–) treatment with 10 μM RA for 24 hours. Bars, numbers of RXRA-PGC1α interactions per cell. Blue fluorescence, 4′,6-diamidino-2-phenylindole (DAPI) nucleic acid stain; $n = 5$ independent experiments, at least 1000 cells counted per experiment. The data are shown as means ± SD. $^*P < 0.05$ compared with untreated cells by Student's t test. (**B**) qRT-PCR analysis of OXPHOS genes in the indicated cells expressing FKBP-RXRA and FRB treated with RA with or without 1 nM rapamycin (RM) for 20 min. The relative mRNA abundances of the indicated OXPHOS genes were measured; $n = 5$ independent experiments. The data are normalized to that of GAPDH and are shown as means ± SD. $^*P < 0.05$ by two-way ANOVA with Bonferroni correction.

in RXRA mRNA abundance in response to ascorbic acid treatment (Fig. 5B and fig. S4A). This may indicate that there is a threshold amount of ROS required to affect RXRA abundance (Fig. 5B).

In neonatal rat cardiomyocytes, the reduction of RXRA abundance by ROS is mediated by a pathway involving JNK (*11*). Thus, we examined the effect of a JNK inhibitor, SP600125 (anthrapyrazolone), on the RXRA abundance. In M cells, inhibition of JNK activity restored the mRNA abundance and increased the protein abundances of RXRA to the amounts in control W cells, indicating that the JNK activity contributed to the reduction of RXRA abundance (Fig. 5C and fig. S4B). Consistent with the lack of effect of antioxidants, inhibition of JNK activity did not alter RXRA mRNA or protein abundance in H cells. Consistent with ROS and JNK participating in the same pathway in the reduction of RXRA, W cells exposed to the ROS hydrogen peroxide exhibited reduced RXRA transcript and protein abundance, and this reduction was partially alleviated by inhibition of JNK activity (fig. S4C).

To examine whether OXPHOS dysfunction caused by mitochondrial poisons also reduced RXRA abundance and involved a pathway with ROS and JNK, we treated W cells with one of three OXPHOS inhibitors—rotenone, antimycin A, or oligomycin—which disrupt the activities of OXPHOS complexes I, III, and V, respectively, leading to OXPHOS

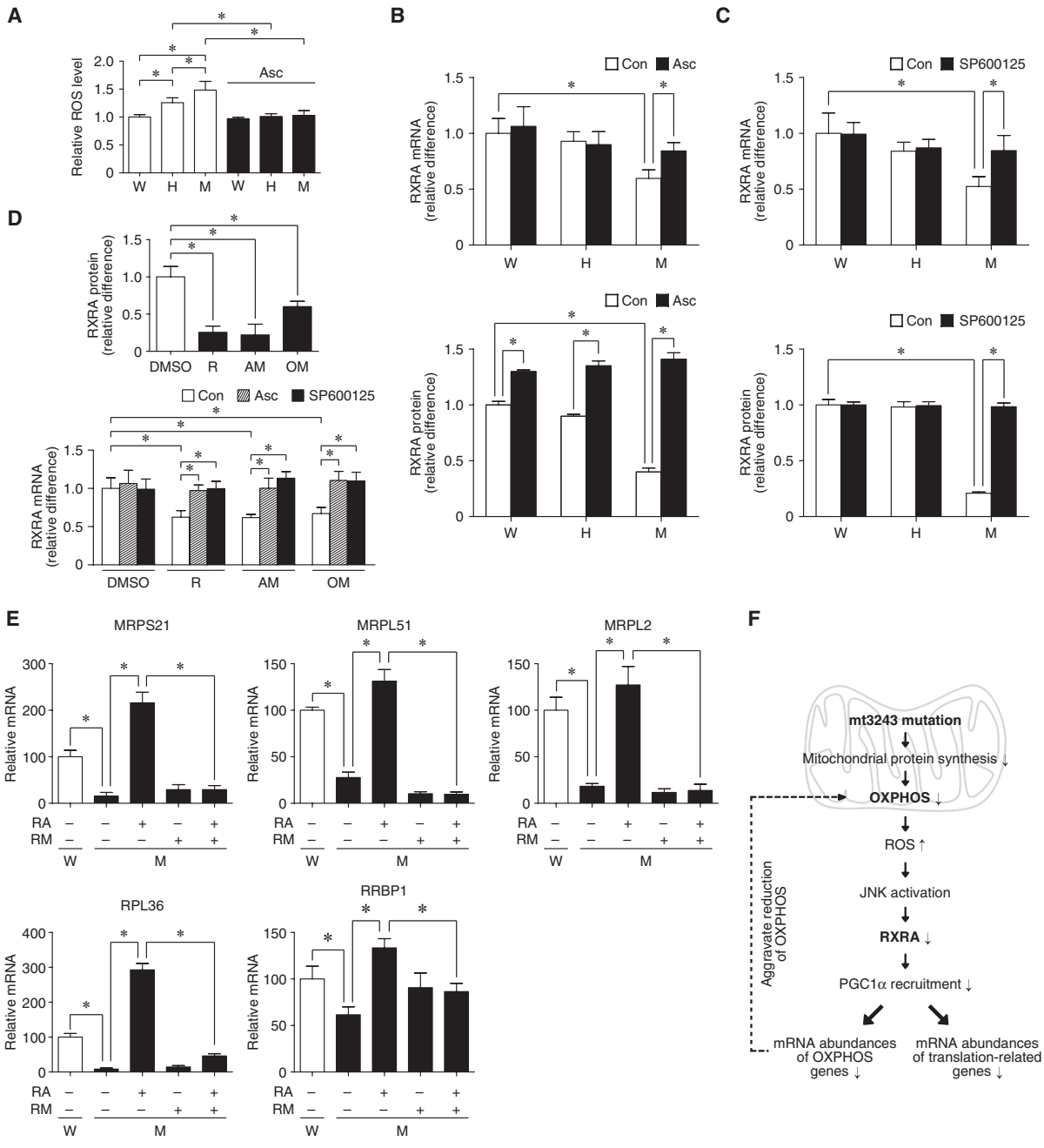

Fig. 5. Decrease of RXRA abundance through JNK activated by ROS. (**A**) Relative ROS amounts in the three types of cybrid cells; $n = 3$ independent experiments. *$P < 0.05$ by two-way ANOVA with Bonferroni correction. (**B**) qRT-PCR and Western blotting analyses of RXRA in three types of cells in the presence or absence of 5 mM ascorbic acid (Asc) for 1 hour. See also fig. S4A; $n = 5$ for qRT-PCR and $n = 3$ for Western blotting independent experiments. *$P < 0.05$ by two-way ANOVA with Bonferroni correction. (**C**) qRT-PCR and Western blotting analyses of RXRA in three types of cells in the presence or absence of 10 μM SP600125 for 1 hour. See also fig. S4B; $n = 5$ for qRT-PCR and $n = 3$ for Western blotting independent experiments. *$P < 0.05$ by two-way ANOVA with Bonferroni correction. (**D**) Effects of OXPHOS inhibitors on RXRA abundance. Upper, Western blotting analysis of RXRA in W cells after the treatment of dimethyl sulfoxide (DMSO), 3 μM rotenone (R), 15 μM antimycin A (AM), or 12 μM oligomycin (OM) for 18 hours; $n = 3$ independent experiments. *$P < 0.05$ by one-way ANOVA with Bonferroni correction. Lower, the relative mRNA abundance after the treatment of Asc or SP600125 was measured in cells exposed to DMSO or the indicated OXPHOS inhibitors; $n = 5$ independent experiments. *$P < 0.05$ by two-way ANOVA with Bonferroni correction. (**E**) qRT-PCR analysis of translation-related genes in cells expressing FKBP-RXRA and FRB treated with RA with or without 1 nM rapamycin (RM) for 20 min; $n = 5$ independent experiments. *$P < 0.05$ by two-way ANOVA with Bonferroni correction. (**F**) A model for a retrograde signaling pathway regulating mRNA abundance of both OXPHOS and translation-related genes. Transcript abundance was normalized to that of GAPDH (B to E). The data in (A) to (E) were expressed as means ± SD.

dysfunctions. Exposure of the W cells to any of the OXPHOS inhibitors resulted in a significant reduction in RXRA mRNA and reduced protein abundance. The effects were prevented by the addition of ascorbic acid to reduce ROS or a JNK inhibitor (Fig. 5D and fig. S4D). Thus, these data indicated that mRNA abundance of RXRA is negatively regulated by JNK activated by ROS, which was induced by mitochondrial dysfunction due to the presence of the mt3243 mutation or the addition of OXPHOS inhibitors.

Regulation of translation-related genes by the RXRA retrograde signaling pathway

Processes classified as translation were among those affected by the presence of the mt3243 mutation (Fig. 2C). Among the 2404 DEGs, 92 genes were classified as involved in translation (table S9). Among the 92 translation-associated genes, 44 were included in C17 and had decreased expression in M cells (Fig. 2B). The network model (Fig. 2E) revealed that translation can also be regulated by the RXRA-PGC1α complex. Gene expression analysis of RA-treated M cells showed that 13 of the 44 translation-related genes in C17 were restored in their mRNA abundances by RA treatment (Fig. 3E). To confirm the gene expression data, we selected 5 genes from the 13 genes and showed that in the rapamycin-induced sequestration assay with cells expressing FKBP-RXRA and FRB, induction of these genes by RA was prevented, suggesting that the RXRA-PGC1α interaction was required in their RA-mediated expression (Fig. 5E). Thus, all these data are consistent with the model that RXRA with PGC1α regulates nuclear-encoded genes involved in cytosolic and mitochondrial translation, in addition to OXPHOS genes, and that this is mediated by a pathway activated in response to mitochondrial dysfunction caused by the presence of the mt3243 mutation involving ROS-mediated activation of JNK (Fig. 5F).

DISCUSSION

Mitochondrial retrograde signaling contributes to the alteration of cellular processes related to mitochondrial diseases. Thus, understanding of mitochondrial retrograde signaling pathways is critical to developing therapeutic options to treat diseases caused by mitochondrial disorders. Here, we used a systems approach to analyze the gene expression profiles of cybrid cells carrying the mt3243 mutation, which is associated with complex clinical phenotypes, and matched those profiles to candidate transcriptional regulators. We identified 72 potential TFs that could be involved in retrograde signaling resulting from the mitochondrial dysfunction caused by the mutation. Among genes affected by the mt3243 mutation, we found decreased mRNA abundances of OXPHOS genes, a key pathological feature in mt3243-related diseases (*14*–*16*), and translation-related genes. We provided evidence for a pathway involving ROS generated by mitochondrial dysfunction, which activated JNK and reduced the abundance of RXRA, which would decrease the formation of the transcriptional regulatory complex RXRA-PGC1 and reduce expression of the OXPHOS and translation-associated genes (Fig. 5F). This pathway formed a transcriptional feedback loop that would further reduce the abundance of OXPHOS enzymes and ribosomal proteins, thereby aggravating mitochondrial dysfunctions (Fig. 5F). Therefore, our gene expression profiling, TF matching, and network-building approach identified retrograde signaling pathways that contributed to the alteration of cellular processes associated with mitochondrial disorders.

The presence of the mt3243 mutation resulted in changes in the mRNA abundances of thousands of genes involved in various cellular processes and potentially targeted by 72 TFs. Although 26 of the 72 TFs, such as CREB (cAMP response element–binding protein) and EGR1, are known to participate in mitochondrial retrograde signaling (tables S1 and S6B), most of the TFs have been rarely studied in association with mitochondrial retrograde signaling. Among the 72 TFs, the expression of 15 was increased or decreased by the presence of the mt3243 mutation. Among the 15, we focused on the role of RXRA in the decrease of OXPHOS genes as a key retrograde signaling TF. There are other interesting TFs that could be involved in mitochondrial retrograde signaling. For example, the mRNA abundance of ETS1, a TF associated with cancers, was increased by the presence of the mt3243 mutation (Fig. 2D). ETS1 regulates hypoxia-inducible genes and also key enzymes involved in glycolysis, fatty acid metabolism, and antioxidant defense in cancer cells (*31*, *32*). Our data indicated a potential link between ETS1 and several mitochondrial processes perturbed by the mt3243 mutation. In addition to the 15 identified in the 72 candidate TFs, the mRNA abundances of another 165 TFs (including FOXO1 and FOXO3) were altered by the presence of the mt3243 mutation (table S10), although they were not selected as mitochondrial retrograde signaling TF candidates, which may be due to the lack of information about their targets. Thus, additional study of these TFs, the expression of which is altered by the presence of the mt3243 mutation, may further extend the list of potential mitochondrial retrograde signaling TFs and reveal their associated retrograde signaling pathways and their roles in controlling the mt3243-related cellular processes and clinical phenotypes.

In conclusion, we show that the approach of transcriptional profiling, combined with matching regulated gene targets with TFs and then construction of regulatory networks, provides an effective method to systematically identify mitochondrial retrograde signaling TFs and their associated pathways activated by mitochondrial dysfunctions. Understanding of these retrograde signaling pathways that contribute to the alteration of processes related to mitochondrial diseases can help discover strategies for preventing the mitochondrial diseases for which there are currently no therapeutic options.

MATERIALS AND METHODS

Cell culture and platelet-mediated transformation of human mtDNA-lacking cells

The rho^0 cells derived from human 143B osteosarcoma cells rendered defective in thymidine kinase activity by long-term exposure to ethidium bromide were a gift from Y.-H. Wei from the National Yang-Ming University in Taiwan. The cells were grown in Dulbecco's modified Eagle's medium (DMEM) supplemented with 5-bromo-2′-deoxyuridine (100 mg/ml) (Sigma-Aldrich), uridine (50 μg/ml) (Sigma-Aldrich), and 10% fetal bovine serum (FBS). Southern blot analysis and PCR amplification of mtDNA target sequences confirmed the absence of residual mtDNA. With the use of platelets as mtDNA donors, cybrid cells were produced as described previously (*33*). Briefly, the platelet-rich fraction was separated by centrifugation from the blood sample of a diabetic patient with sensorineural hearing loss and harboring mutated mitochondrial tRNA^{Leu} (A3243G), and 143B rho^0 cells were added to this fraction. Fusion was carried out in the presence of 42% polyethylene glycol 1500 (Sigma-Aldrich). By limiting dilution of cellular fusion products, we isolated cybrid clones with 3243A homoplasmy (W), 3243G homoplasmy (M), and 3243A/G heteroplasmy (H). These clones were confirmed by PCR-RFLP analysis and direct sequencing. To assure a complete repopulation of mtDNA, we carried out functional assessment of the selected clones after 3 months of successive subcultivation. For consistent analysis, we used cybrid cells in passages 16 to 18.

To determine the amount of mutant DNA in the cybrid cells, we mixed wild-type and mutant DNA to generate heteroplasmic samples of 0, 20, 40, 60, 80, and 100%; quantified the intensities of the band in individual heteroplasmic samples by densitometry; and then generated a standard

curve with the mutant DNA percentages and their intensities. Using the standard curve, we quantified the mutant DNA percentage for the measured intensity in cybrid cells.

Measurement of oxygen consumption

The suspension of 1×10^5 cells in DMEM was added to 96-well BD Oxygen Biosensor System plate (BD Biosciences). The plate was incubated for 30 min at 37°C in 5% CO_2 incubator. The oxygen consumption was measured by VICTOR3 Multilabel Plate Reader (PerkinElmer) with an excitation wavelength of 485 nm and an emission wavelength of 630 nm.

Assays for ATP production and cytochrome c oxidase

We seeded 1×10^4 cells into microplates and incubated them overnight. The ATP abundance was measured with the ATPLite kit (PerkinElmer) according to the manufacturer's instruction. Cytochrome c oxidase activity was assayed as described in (*34*). The activity was performed by Beckman DU 650 spectrophotometer.

Microarray experiment

Gene expression profiles of cybrid cells were generated with HumanHT-12 v3 BeadChip (Illumina), which includes 49,896 probes corresponding to 25,202 annotated genes. According to the Illumina protocols, three biological triplicates of each type of cybrid cells were analyzed. Total RNA (500 ng) was isolated from cybrid cells with the RNeasy Mini Kit (Qiagen GmbH). RNA integrity number was in the range of 9.2 to 10 when measured with an Agilent 2100 Bioanalyzer. RNA was reversely transcribed and amplified with the Illumina TotalPrep RNA Amplification Kit (Ambion). In vitro transcription was then carried out to prepare complementary RNA (cRNA). The cRNAs were hybridized to the array and then labeled with Cy3-Streptavidin (Amersham Bioscience). The fluorescent signal on the array was measured with the BeadStation 500 System (Illumina).

Statistical analysis of gene expression data

The probe intensities from the arrays were converted to $\log_2$ intensities. The $\log_2$ intensities were then normalized with the quantile normalization method (*35*). The probes were annotated with Lumi 1.8.3. The expressed genes were identified as previously described (*36*). To identify DEGs, integrative statistical hypothesis testing was performed (*36*). Briefly, Student's *t* test and $\log_2$ median ratio test were performed to compute *T* values and $\log_2$ median ratios for all the genes; empirical distributions of the null hypothesis (that is, a gene is not differential expressed) were estimated by performing all possible combinations of random permutations of samples and then by applying the Gaussian kernel density estimation method to *T* values and $\log_2$ median ratios resulted from the random permutations (*37*); the adjusted *P* values of each gene for the individual tests were computed by the two-tailed test with the empirical null distribution; the *P* values from the two tests were then combined with the Stouffer's method (*38*); FDRs for the combined *P* values were then computed with the Storey method (*39*); and an initial set of the DEGs were identified as the genes with FDR ≤ 0.05. Among the initial set of DEGs with FDR ≤ 0.05, we then selected a final set of DEGs that have absolute $\log_2$ fold changes larger than a cutoff (0.55; 1.46-fold change), the mean of 0.5th and 99.5th percentiles of the null distribution of $\log_2$ fold changes.

Enrichment analysis of GO Biological Processes

For the enrichment analysis of GO Biological Processes for a list of genes, we obtained a list of the genes to be used in the analysis for each GO Biological Process. For OXPHOS, we used the genes obtained from both the "oxidative phosphorylation" GO term (GO:0006119) and the "oxidative phosphorylation" KEGG pathway (hsa00190), which increased the set of genes for the analysis. For the other GO Biological Processes, we used the genes obtained from the corresponding GO terms only. With the use of these lists of the genes for GO Biological Processes, *P* value was calculated for the genes in individual clusters (Fig. 2B) as described in DAVID (*17*). Finally, GO Biological Processes enriched within the genes in each cluster were identified as the ones with $P < 0.05$.

Identification of potential retrograde signaling TFs

To identify potential retrograde signaling TFs, we collected 223,665 TF-target interactions (table S5). Using the TF-target information, for each TF, we counted the number of targets in the 12 clusters and then selected 72 TFs that had statistically significant numbers of targets (FDR < 0.01) in the 12 DEG clusters with the following method: For each TF, we first randomly sampled 100,000 times the same number of genes as that of the DEGs in each cluster from the pool of genes spotted on the array and then counted the number of targets of the TF in the randomly sampled genes; for each cluster, we then estimated an empirical distribution for the numbers of targets of the TF from the 100,000 random samplings with Gaussian kernel density estimation (*37*); and with the empirical distribution, we computed an FDR for the observed number of targets of the TF in the corresponding cluster with the Storey method (*39*). This procedure results in FDRs for each TF in the 12 clusters. We then selected 72 potential retrograde signaling TF candidates with the following criteria: FDR < 0.01 in more than four different clusters (25% of 12 clusters), and where w_i is the number of DEGs in cluster *i* divided by the total number of 2404 DEGs, and I_i is 1 if FDR < 0.01 in cluster *i*, but 0 otherwise. These stringent criteria would result in a list of reliable TF candidates, reducing the rate of false positives.

siRNA injection

Cells were transiently transfected with the OneDrop Microporator MP Kit (Invitrogen) according to the manufacturer's instructions after siRNA synthesis. Briefly, 1×10^5 cells were resuspended in 100 μl of resuspension buffer and transfected with 100 nM siRNA (RXRA; Thermo Scientific Dharmacon RNAi Technologies, L-003443-00-0005). After transfection, the cells were transferred to a six-well plate (Nunc) containing fresh prewarmed DMEM and maintained for 72 hours at 37°C and 5% CO_2. Then, the mRNA abundance for specific transcripts was monitored by qRT-PCR.

Immunocytochemistry

Cells were grown on Lab-Tek II Chamber Slide (Nunc) and treated with RA for 24 hours. The cells were rinsed in phosphate-buffered saline (PBS), fixed in methanol for 20 min, and rinsed again in PBS. Cells were incubated overnight with antibodies (table S11) against RXRA (rabbit, Santa Cruz, sc-553) or PGC1α (mouse, Santa Cruz, sc-13067) and a mitochondrial marker (mouse, Abcam, ab3298) at 4°C. Cells were rinsed with PBS and then incubated for 1 hour at room temperature with secondary antibodies, Alexa Fluor 555 donkey anti-rabbit immunoglobulin G (IgG) (Invitrogen, A31572) and IgG (Invitrogen, A21427). See concentration information in table S11. For counterstaining of the nucleus, cells were incubated with DAPI (1 μg/ml; Sigma-Aldrich) for 40 s. After washing with PBS, coverslips were mounted on glass slides, with VECTASHIELD mounting media (Vector Laboratories), and analyzed with LSM 710 confocal microscope (Carl Zeiss).

Proximity ligation assay

PLA was performed in each type of cybrid cells with and without the RA treatment to visualize the RXRA-PGC1α interactions. Cells were washed with chilled PBS and incubated overnight with antibodies (table S11) against RXRA (rabbit, Santa Cruz, sc-553) or PGC1α (mouse, Santa

Cruz, sc-13067) at 4°C. Proximity ligation was performed, according to the manufacturer's protocol, with the Duolink detection kit (Olink Bioscience). Hoechst staining was performed during the detection reaction to visualize nuclei. Specimens were mounted with VECTASHIELD mounting media (Vector Laboratories) and analyzed with LSM 710 confocal microscope. The number of in situ PLA signals per cell was counted by semiautomated image analysis with BlobFinderV3.0.

FRB assay

Cells were transiently transfected with the OneDrop Microporator MP Kit (Invitrogen) according to the manufacturer's instructions after plasmid DNA synthesis. For qRT-PCR, 5×10^5 cells were resuspended in 100 μl of resuspension buffer and transfected with 10 μg of plasmids containing FKBP-RXRA and FRB. For PLA assay, 1×10^4 cells were resuspended in 10 μl of resuspension buffer, placed in a well of a glass-bottomed dish (Nunc) with fresh prewarmed DMEM, transfected with 1 μg of each plasmid containing FKBP-RXRA and FRB, and maintained for 72 hours at 37°C and 5% CO_2. Then, the cells were incubated at room temperature for 20 min with 1 nM rapamycin, and the interaction between RXRA and PGC1α was measured by PLA assay. The mRNA abundance of specific transcripts was monitored by qRT-PCR.

Exposure of cells to RA, ascorbic acid, JNK inhibitor, or mitochondrial poisons

Cells were grown in DMEM with high glucose supplemented with 10% FBS and incubated at 37°C and 5% CO_2. The cells were treated with 10 μM 9-*cis*-RA (Sigma, R4643) for 24 hours. The cells were exposed to 5 mM ascorbic acid (Sigma-Aldrich, A4403) or 10 μM SP600125 (JNK inhibitor, Sigma-Aldrich, S5567) for 1 hour. For cells exposed to ascorbic acid or SP600125 and mitochondrial poisons, the cells were treated for 1 hour with 5 mM ascorbic acid or 10 μM SP600125, and then 3 μM rotenone (Sigma-Aldrich, R8875), 15 μM antimycin A (Sigma-Aldrich, A8674), or 12 μM oligomycin (Sigma-Aldrich, O4876) was added and the cells were incubated for 18 hours at 37°C and 5% CO_2. The cells were then harvested for Western blotting and qRT-PCR.

Quantitative RT-PCR

RNA was isolated with TRIzol reagent (Invitrogen Corp.), pooled, and then subjected to first-strand complementary DNA synthesis with Reverse Transcription System (Takara) according to the manufacturer's protocol. qPCR primer sequences were designed by Primer Express (Applied Biosystems; table S12). The qRT-PCR was performed with 7900HT Fast Real-Time PCR System (Applied Biosystems). Threshold cycle number and reaction efficiency were determined with the software in GeneAmp 7900HT Sequence Detection System (PerkinElmer Corp.). The following profile was used: at 95°C for 10 min, and then 40 cycles of 95°C for 15 s and 60°C for 60 s. Expression was normalized by that of GAPDH.

Western blotting analysis

Cell lysates (50 μg) were subjected to 12% SDS–polyacrylamide gel electrophoresis and transferred onto nitrocellulose membranes. The membranes were incubated with primary antibodies. After washing, the blots were incubated with horseradish peroxidase–conjugated secondary antibodies. The blots were developed with SuperSignal West Pico Chemiluminescent Substrate (Pierce). The primary antibodies used in this study are listed in table S11.

Measurement of intracellular ROS

Cells were treated with 2′,7′-dichlorohydro-fluorescein diacetate (Invitrogen) in DMEM supplemented with 10% FBS for 15 min. Fluorescence was detected by VICTOR3 Multilabel Plate Reader (PerkinElmer) with an excitation wavelength of 485 nm and an emission wavelength of 535 nm.

Statistical analysis

All data were normalized by the mean values of the replicate data in untreated W cells (control) and expressed as means ± SD. For comparisons of two groups (for example, with and without siRNA treatments), we used the two-tailed Student's *t* test. Also, for comparisons among multiple groups of one variable (for example, O_2 consumption, ATP content, mRNA, and protein abundances of RXRA in W, H, and M cells), we used one-way ANOVA with Bonferroni correction as a post hoc test. Finally, for comparisons among multiple groups of two variables (for example, mutational load and treatments), we used two-way ANOVA with Bonferroni correction as a post hoc test. The criterion of significance was set as $P < 0.05$ in all cases.

SUPPLEMENTARY MATERIALS

www.sciencesignaling.org/cgi/content/full/6/264/rs4/DC1

Fig. S1. Association of DEGs with cellular processes and genes that have been previously reported to be affected by the mt3243 mutation.

Fig. S2. Differential expression of TFs known to participate in mitochondrial retrograde signaling.

Fig. S3. Knockdown of RXRA using siRNA.

Fig. S4. Regulation of mRNA and protein abundances of RXRA through JNK activated by ROS.

Table S1. Mitochondria-to-nucleus retrograde signaling mediators, signaling pathways, and their downstream TFs.

Table S2. Organizing the 2404 DEGs into clusters and their differential expression patterns among the three types of cells.

Table S3. The lists of the genes included in the individual clusters.

Table S4. GO Biological Processes enriched in the DEGs in the individual clusters.

Table S5. TF-target interactions collected from the six databases.

Table S6. Seventy-two TFs that could potentially be involved in retrograde signaling induced by the mt3243 mutation.

Table S7. The OXPHOS genes differentially expressed in cells containing the mt3243 mutation.

Table S8. One hundred sixty-three DEGs that showed an increase in mRNA abundances in 3243G M cells by the RA treatment.

Table S9. The translation-related genes differentially expressed in cells containing the mt3243 mutation.

Table S10. One hundred eighty TFs that showed altered mRNA abundance in cells containing the mt3243 mutation.

Table S11. Primary antibodies used for Western blotting analysis and immunofluorescence analysis.

Table S12. Primer sequences used in qRT-PCR analysis.

REFERENCES AND NOTES

1. T. Finkel, N. J. Holbrook, Oxidants, oxidative stress and the biology of ageing. *Nature* **408**, 239–247 (2000).
2. R. G. Allen, M. Tresini, Oxidative stress and gene regulation. *Free Radic. Biol. Med.* **28**, 463–499 (2000).
3. L. W. Finley, M. C. Haigis, The coordination of nuclear and mitochondrial communication during aging and calorie restriction. *Ageing Res. Rev.* **8**, 173–188 (2009).
4. M. T. Ryan, N. J. Hoogenraad, Mitochondrial-nuclear communications. *Annu. Rev. Biochem.* **76**, 701–722 (2007).
5. Z. Liu, R. A. Butow, Mitochondrial retrograde signaling. *Annu. Rev. Genet.* **40**, 159–185 (2006).
6. R. A. Butow, N. G. Avadhani, Mitochondrial signaling: The retrograde response. *Mol. Cell* **14**, 1–15 (2004).
7. D. Hwang, I. Y. Lee, H. Yoo, N. Gehlenborg, J. H. Cho, B. Petritis, D. Baxter, R. Pitstick, R. Young, D. Spicer, N. D. Price, J. G. Hohmann, S. J. Dearmond, G. A. Carlson, L. E. Hood, A systems approach to prion disease. *Mol. Syst. Biol.* **5**, 252 (2009).
8. M. Crimi, A. Bordoni, G. Menozzi, L. Riva, F. Fortunato, S. Galbiati, R. Del Bo, U. Pozzoli, N. Bresolin, G. P. Comi, Skeletal muscle gene expression profiling in mitochondrial disorders. *FASEB J.* **19**, 866–868 (2005).
9. G. M. Janssen, J. A. Maassen, J. M. van Den Ouweland, The diabetes-associated 3243 mutation in the mitochondrial $tRNA^{Leu(UUR)}$ gene causes severe mitochondrial dysfunction without a strong decrease in protein synthesis rate. *J. Biol. Chem.* **274**, 29744–29748 (1999).

10. A. Chomyn, A. Martinuzzi, M. Yoneda, A. Daga, O. Hurko, D. Johns, S. T. Lai, I. Nonaka, C. Angelini, G. Attardi, MELAS mutation in mtDNA binding site for transcription termination factor causes defects in protein synthesis and in respiration but no change in levels of upstream and downstream mature transcripts. *Proc. Natl. Acad. Sci. U.S.A.* **89**, 4221–4225 (1992).
11. A. B. Singh, R. S. Guleria, I. T. Nizamutdinova, K. M. Baker, J. Pan, High glucose-induced repression of RAR/RXR in cardiomyocytes is mediated through oxidative stress/JNK signaling. *J. Cell. Physiol.* **227**, 2632–2644 (2012).
12. P. Delerive, Y. Wu, T. P. Burris, W. W. Chin, C. S. Suen, PGC-1 functions as a transcriptional coactivator for the retinoid X receptors. *J. Biol. Chem.* **277**, 3913–3917 (2002).
13. J. M. van den Ouweland, P. Maechler, C. B. Wollheim, G. Attardi, J. A. Maassen, Functional and morphological abnormalities of mitochondria harbouring the $tRNA^{Leu(UUR)}$ mutation in mitochondrial DNA derived from patients with maternally inherited diabetes and deafness (MIDD) and progressive kidney disease. *Diabetologia* **42**, 485–492 (1999).
14. R. W. Taylor, D. M. Turnbull, Mitochondrial DNA mutations in human disease. *Nat. Rev. Genet.* **6**, 389–402 (2005).
15. D. C. Wallace, Mitochondrial diseases in man and mouse. *Science* **283**, 1482–1488 (1999).
16. Y. H. Wei, S. B. Wu, Y. S. Ma, H. C. Lee, Respiratory function decline and DNA mutation in mitochondria, oxidative stress and altered gene expression during aging. *Chang Gung Med. J.* **32**, 113–132 (2009).
17. D. W. Huang, B. T. Sherman, R. A. Lempicki, Systematic and integrative analysis of large gene lists using DAVID bioinformatics resources. *Nat. Protoc.* **4**, 44–57 (2009).
18. F. Reinecke, J. A. Smeitink, F. H. van der Westhuizen, OXPHOS gene expression and control in mitochondrial disorders. *Biochim. Biophys. Acta* **1792**, 1113–1121 (2009).
19. S. R. Danielson, V. Carelli, G. Tan, A. Martinuzzi, A. H. Schapira, M. L. Savontaus, G. A. Cortopassi, Isolation of transcriptomal changes attributable to LHON mutations and the cybridization process. *Brain* **128**, 1026–1037 (2005).
20. M. F. Marusich, B. H. Robinson, J. W. Taanman, S. J. Kim, R. Schillace, J. L. Smith, R. A. Capaldi, Expression of mtDNA and nDNA encoded respiratory chain proteins in chemically and genetically-derived Rho0 human fibroblasts: A comparison of subunit proteins in normal fibroblasts treated with ethidium bromide and fibroblasts from a patient with mtDNA depletion syndrome. *Biochim. Biophys. Acta* **1362**, 145–159 (1997).
21. A. Čížková, V. Stránecký, R. Ivánek, H. Hartmannová, L. Nosková, L. Piherová, M. Tesařová, H. Hansíková, T. Honzík, J. Zeman, P. Divina, A. Potocká, J. Paul, W. Sperl, J. A. Mayr, S. Seneca, J. Houštěk, S. Kmoch, Development of a human mitochondrial oligonucleotide microarray (h-MitoArray) and gene expression analysis of fibroblast cell lines from 13 patients with isolated F_1F_o ATP synthase deficiency. *BMC Genomics* **9**, 38 (2008).
22. P. Puigserver, Z. Wu, C. W. Park, R. Graves, M. Wright, B. M. Spiegelman, A cold-inducible coactivator of nuclear receptors linked to adaptive thermogenesis. *Cell* **92**, 829–839 (1998).
23. Z. Wu, P. Puigserver, U. Andersson, C. Zhang, G. Adelmant, V. Mootha, A. Troy, S. Cinti, B. Lowell, R. C. Scarpulla, B. M. Spiegelman, Mechanisms controlling mitochondrial biogenesis and respiration through the thermogenic coactivator PGC-1. *Cell* **98**, 115–124 (1999).
24. J. St-Pierre, J. Lin, S. Krauss, P. T. Tarr, R. Yang, C. B. Newgard, B. M. Spiegelman, Bioenergetic analysis of peroxisome proliferator-activated receptor γ coactivators 1α and 1β (PGC-1α and PGC-1β) in muscle cells. *J. Biol. Chem.* **278**, 26597–26603 (2003).
25. R. A. Heyman, D. J. Mangelsdorf, J. A. Dyck, R. B. Stein, G. Eichele, R. M. Evans, C. Thaller, 9-cis retinoic acid is a high affinity ligand for the retinoid X receptor. *Cell* **68**, 397–406 (1992).
26. X. K. Zhang, J. Lehmann, B. Hoffmann, M. I. Dawson, J. Cameron, G. Graupner, T. Hermann, P. Tran, M. Pfahl, Homodimer formation of retinoid X receptor induced by 9-*cis* retinoic acid. *Nature* **358**, 587–591 (1992).
27. Y. W. Lin, L. M. Lien, T. S. Yeh, H. M. Wu, Y. L. Liu, R. H. Hsieh, 9-cis retinoic acid induces retinoid X receptor localized to the mitochondria for mediation of mitochondrial transcription. *Biochem. Biophys. Res. Commun.* **377**, 351–354 (2008).
28. R. Acin-Perez, B. Hoyos, F. Zhao, V. Vinogradov, D. A. Fischman, R. A. Harris, M. Leitges, N. Wongsiriroj, W. S. Blaner, G. Manfredi, U. Hammerling, Control of oxidative phosphorylation by vitamin A illuminates a fundamental role in mitochondrial energy homoeostasis. *FASEB J.* **24**, 627–636 (2010).
29. C. D. Berdanier, H. B. Everts, C. Hermoyian, C. E. Mathews, Role of vitamin A in mitochondrial gene expression. *Diabetes Res. Clin. Pract.* **54**, S11–S27 (2001).
30. W. D. Heo, T. Inoue, W. S. Park, M. L. Kim, B. O. Park, T. J. Wandless, T. Meyer, $PI(3,4,5)P_3$ and $PI(4,5)P_2$ lipids target proteins with polybasic clusters to the plasma membrane. *Science* **314**, 1458–1461 (2006).
31. K. Salnikow, O. Aprelikova, S. Ivanov, S. Tackett, M. Kaczmarek, A. Karaczyn, H. Yee, K. S. Kasprzak, J. Niederhuber, Regulation of hypoxia-inducible genes by ETS1 transcription factor. *Carcinogenesis* **29**, 1493–1499 (2008).
32. M. L. Verschoor, L. A. Wilson, C. P. Verschoor, G. Singh, Ets-1 regulates energy metabolism in cancer cells. *PLoS One* **5**, e13565 (2010).
33. A. Chomyn, Platelet-mediated transformation of human mitochondrial DNA-less cells. *Methods Enzymol.* **264**, 334–339 (1996).
34. E. A. Madden, B. Storrie, The preparative isolation of mitochondria from Chinese hamster ovary cells. *Anal. Biochem.* **163**, 350–357 (1987).
35. B. M. Bolstad, R. A. Irizarry, M. Astrand, T. P. Speed, A comparison of normalization methods for high density oligonucleotide array data based on variance and bias. *Bioinformatics* **19**, 185–193 (2003).
36. H. J. Lee, J. E. Suk, C. Patrick, E. J. Bae, J. H. Cho, S. Rho, D. Hwang, E. Masliah, S. J. Lee, Direct transfer of α-synuclein from neuron to astroglia causes inflammatory responses in synucleinopathies. *J. Biol. Chem.* **285**, 9262–9272 (2010).
37. A. W. Bowman, A. Azzalini, *Applied Smoothing Techniques for Data Analysis: The Kernel Approach with S-Plus Illustrations* (Clarendon Press, Oxford, 1997).
38. D. Hwang, A. G. Rust, S. Ramsey, J. J. Smith, D. M. Leslie, A. D. Weston, P. de Atauri, J. D. Aitchison, L. Hood, A. F. Siegel, H. Bolouri, A data integration methodology for systems biology. *Proc. Natl. Acad. Sci. U.S.A.* **102**, 17296–17301 (2005).
39. J. D. Storey, R. Tibshirani, Statistical significance for genomewide studies. *Proc. Natl. Acad. Sci. U.S.A.* **100**, 9440–9445 (2003).
40. G. Biswas, O. A. Adebanjo, B. D. Freedman, H. K. Anandatheerthavarada, C. Vijayasarathy, M. Zaidi, M. Kotlikoff, N. G. Avadhani, Retrograde Ca^{2+} signaling in C2C12 skeletal myocytes in response to mitochondrial genetic and metabolic stress: A novel mode of inter-organelle crosstalk. *EMBO J.* **18**, 522–533 (1999).
41. G. Biswas, H. K. Anandatheerthavarada, M. Zaidi, N. G. Avadhani, Mitochondria to nucleus stress signaling: A distinctive mechanism of NFκB/Rel activation through calcineurin-mediated inactivation of IκBβ. *J. Cell Biol.* **161**, 507–519 (2003).
42. T. Arnould, S. Vankoningsloo, P. Renard, A. Houbion, N. Ninane, C. Demazy, J. Remacle, M. Raes, CREB activation induced by mitochondrial dysfunction is a new signaling pathway that impairs cell proliferation. *EMBO J.* **21**, 53–63 (2002).
43. D. Freyssenet, I. Irrcher, M. K. Connor, M. Di Carlo, D. A. Hood, Calcium-regulated changes in mitochondrial phenotype in skeletal muscle cells. *Am. J. Physiol. Cell Physiol.* **286**, C1053–C1061 (2004).
44. Q. Zhao, J. Wang, I. V. Levichkin, S. Stasinopoulos, M. T. Ryan, N. J. Hoogenraad, A mitochondrial specific stress response in mammalian cells. *EMBO J.* **21**, 4411–4419 (2002).
45. B. Mellström, M. Savignac, R. Gomez-Villafuertes, J. R. Naranjo, Ca^{2+}-operated transcriptional networks: Molecular mechanisms and in vivo models. *Physiol. Rev.* **88**, 421–449 (2008).
46. H. Wu, S. B. Kanatous, F. A. Thurmond, T. Gallardo, E. Isotani, R. Bassel-Duby, R. S. Williams, Regulation of mitochondrial biogenesis in skeletal muscle by CaMK. *Science* **296**, 349–352 (2002).
47. I. K. Aggeli, I. Beis, C. Gaitanaki, ERKs and JNKs mediate hydrogen peroxide-induced Egr-1 expression and nuclear accumulation in H9c2 cells. *Physiol. Res.* **59**, 443–454 (2010).
48. C. K. Sen, L. Packer, Antioxidant and redox regulation of gene transcription. *FASEB J.* **10**, 709–720 (1996).
49. K. Nose, M. Shibanuma, K. Kikuchi, H. Kageyama, S. Sakiyama, T. Kuroki, Transcriptional activation of early-response genes by hydrogen peroxide in a mouse osteoblastic cell line. *Eur. J. Biochem.* **201**, 99–106 (1991).
50. D. W. Li, A. Spector, Hydrogen peroxide-induced expression of the proto-oncogenes, *c-jun*, *c-fos* and *c-myc* in rabbit lens epithelial cells. *Mol. Cell. Biochem.* **173**, 59–69 (1997).
51. P. Storz, H. Döppler, A. Toker, Protein kinase D mediates mitochondrion-to-nucleus signaling and detoxification from mitochondrial reactive oxygen species. *Mol. Cell. Biol.* **25**, 8520–8530 (2005).
52. B. Liu, Y. Chen, D. K. St Clair, ROS and p53: A versatile partnership. *Free Radic. Biol. Med.* **44**, 1529–1535 (2008).
53. E. Owusu-Ansah, A. Yavari, S. Mandal, U. Banerjee, Distinct mitochondrial retrograde signals control the G1-S cell cycle checkpoint. *Nat. Genet.* **40**, 356–361 (2008).
54. M. A. Essers, S. Weijzen, A. M. de Vries-Smits, I. Saarloos, N. D. de Ruiter, J. L. Bos, B. M. Burgering, FOXO transcription factor activation by oxidative stress mediated by the small GTPase Ral and JNK. *EMBO J.* **23**, 4802–4812 (2004).
55. T. Nakamura, K. Sakamoto, Forkhead transcription factor FOXO subfamily is essential for reactive oxygen species-induced apoptosis. *Mol. Cell. Endocrinol.* **281**, 47–55 (2008).
56. S. S. Myatt, J. J. Brosens, E. W. Lam, Sense and sensitivity: FOXO and ROS in cancer development and treatment. *Antioxid. Redox Signal.* **14**, 675–687 (2011).
57. H. Sato, M. Sato, H. Kanai, T. Uchiyama, T. Iso, Y. Ohyama, H. Sakamoto, J. Tamura, R. Nagai, M. Kurabayashi, Mitochondrial reactive oxygen species and c-Src play a critical role in hypoxic response in vascular smooth muscle cells. *Cardiovasc. Res.* **67**, 714–722 (2005).
58. Q. Zhou, L. Z. Liu, B. Fu, X. Hu, X. Shi, J. Fang, B. H. Jiang, Reactive oxygen species regulate insulin-induced VEGF and HIF-1α expression through the activation of p70S6K1 in human prostate cancer cells. *Carcinogenesis* **28**, 28–37 (2007).
59. M. E. Martin, Y. Chinenov, M. Yu, T. K. Schmidt, X. Y. Yang, Redox regulation of GA-binding protein-α DNA binding activity. *J. Biol. Chem.* **271**, 25617–25623 (1996).
60. H. B. Suliman, M. S. Carraway, K. E. Welty-Wolf, A. R. Whorton, C. A. Piantadosi, Lipopolysaccharide stimulates mitochondrial biogenesis via activation of nuclear respiratory factor-1. *J. Biol. Chem.* **278**, 41510–41518 (2003).

61. C. A. Piantadosi, H. B. Suliman, Mitochondrial transcription factor A induction by redox activation of nuclear respiratory factor 1. *J. Biol. Chem.* **281**, 324–333 (2006).
62. W. J. Lee, M. Kim, H. S. Park, H. S. Kim, M. J. Jeon, K. S. Oh, E. H. Koh, J. C. Won, M. S. Kim, G. T. Oh, M. Yoon, K. U. Lee, J. Y. Park, AMPK activation increases fatty acid oxidation in skeletal muscle by activating PPARα and PGC-1. *Biochem. Biophys. Res. Commun.* **340**, 291–295 (2006).
63. S. Jäger, C. Handschin, J. St-Pierre, B. M. Spiegelman, AMP-activated protein kinase (AMPK) action in skeletal muscle via direct phosphorylation of PGC-1α. *Proc. Natl. Acad. Sci. U.S.A.* **104**, 12017–12022 (2007).
64. E. L. Greer, P. R. Oskoui, M. R. Banko, J. M. Maniar, M. P. Gygi, S. P. Gygi, A. Brunet, The energy sensor AMP-activated protein kinase directly regulates the mammalian FOXO3 transcription factor. *J. Biol. Chem.* **282**, 30107–30119 (2007).
65. K. Inoki, T. Zhu, K. L. Guan, TSC2 mediates cellular energy response to control cell growth and survival. *Cell* **115**, 577–590 (2003).
66. R. J. Shaw, N. Bardeesy, B. D. Manning, L. Lopez, M. Kosmatka, R. A. DePinho, L. C. Cantley, The LKB1 tumor suppressor negatively regulates mTOR signaling. *Cancer Cell* **6**, 91–99 (2004).
67. D. M. Gwinn, D. B. Shackelford, D. F. Egan, M. M. Mihaylova, A. Mery, D. S. Vasquez, B. E. Turk, R. J. Shaw, AMPK phosphorylation of raptor mediates a metabolic checkpoint. *Mol. Cell* **30**, 214–226 (2008).
68. C. Jiang, Z. Xuan, F. Zhao, M. Q. Zhang, TRED: A transcriptional regulatory element database, new entries and other development. *Nucleic Acids Res.* **35**, D137–D140 (2007).
69. G. D. Bader, D. Betel, C. W. Hogue, BIND: The Biomolecular Interaction Network Database. *Nucleic Acids Res.* **31**, 248–250 (2003).
70. C. Linhart, Y. Halperin, R. Shamir, Transcription factor and microRNA motif discovery: The Amadeus platform and a compendium of metazoan target sets. *Genome Res.* **18**, 1180–1189 (2008).
71. J. Severin, A. M. Waterhouse, H. Kawaji, T. Lassmann, E. van Nimwegen, P. J. Balwierz, M. J. de Hoon, D. A. Hume, P. Caminci, Y. Hayashizaki, H. Suzuki, C. O. Daub, A. R. Forrest, FANTOM4 EdgeExpressDB: An integrated database of promoters, genes, microRNAs, expression dynamics and regulatory interactions. *Genome Biol.* **10**, R39 (2009).
72. A. Subramanian, P. Tamayo, V. K. Mootha, S. Mukherjee, B. L. Ebert, M. A. Gillette, A. Paulovich, S. L. Pomeroy, T. R. Golub, E. S. Lander, J. P. Mesirov, Gene set enrichment analysis: A knowledge-based approach for interpreting genome-wide expression profiles. *Proc. Natl. Acad. Sci. U.S.A.* **102**, 15545–15550 (2005).

Acknowledgments: We thank Y.-H. Wei at the National Yang-Ming University in Taiwan for providing us with the rho^0 cells derived from human 143B osteosarcoma cells. **Funding:** This study was supported by the Korean Ministry of Education, Science and Technology grants from the Converging Research Center Program (2011K000896), Global Frontier Project grant (NRF-M1AXA002-2011-0028392), World Class University program (R31-2008-000-10105-0), 21C Frontier Functional Proteomics Project (FPR08A1-070), and Proteogenomic Research Program. **Author contributions:** D.H., B.L., and K.S.P. designed the project. S.C. and D.H. designed and performed statistical analysis. B.Y.A., K.B., Y.M.C., and B.L. performed the experiments. S.C., K.B., B.Y.A., M.-H.Y., B.L., K.S.P., and D.H. analyzed the data and wrote the paper. All authors provided editorial input. **Competing interests:** The authors declare that they have no competing interests. **Data and materials availability:** Gene expression data used in this study are available from Gene Expression Omnibus database (http://www.ncbi.nlm.nih.gov/gds/) under submission number GSE 27545.

Submitted 29 May 2012
Accepted 1 February 2013
Final Publication 26 February 2013
10.1126/scisignal.2003266
Citation: S. Chae, B. Y. Ahn, K. Byun, Y. M. Cho, M.-H. Yu, B. Lee, D. Hwang, K. S. Park, A systems approach for decoding mitochondrial retrograde signaling pathways. *Sci. Signal.* **6**, rs4 (2013).